Astron. Astrophys. 354, 595–604 (2000)

ASTRONOMY AND ASTROPHYSICS

Spectro-polarimetric interferometry (SPIN) of magnetic stars

K. Rousselet-Perraut[1], **O. Chesneau**[2], **Ph. Berio**[2], **and F. Vakili**[2]

[1] Laboratoire d'Astrophysique UMR UJF/CNRS 5571, Observatoire de Grenoble, B.P. 53, 38041 Grenoble cedex 9, France
[2] Observatoire de la Côte d'Azur, Département Fresnel, CNRS UMR 6528, 06460 Saint Vallier de Thiey, France

Received 8 February 1999 / Accepted 18 November 1999

Abstract. Stellar magnetic fields are usually studied by spectropolarimetric analysis of the Zeeman effect across spectral lines. Such studies are often limited by the net detectable polarization after averaging the small scale magnetic structures over the photospheric disk of the star. In this paper we examine the possibility to use optical long baseline interferometry to overcome this limitation for a partially or fully resolved star which, in the case of the brightest Ap and Bp stars, demands milliarcsecond resolutions achievable at 50 m baselines at least in the visible. We develop a simple geometrical model of magnetic stars from which we derive the intensity maps and their corresponding interferometric observables across Zeeman-split lines. The accuracy of the interferometric signal phase must be better than 0.5° (hence a relative accuracy of 0.1%), which limits the technique to brightest magnetic stars ($m_V \leq 2$) for operating interferometers. Nevertheless, this limiting magnitude can reach $m_K \leq$ 8-10 for 8-m class planned interferometers. These foreseeable possibilities open new areas for studying slowly rotating magnetic stars or those sources possessing complex structures over their visible disk, otherwise undetectable by classical spectropolarimetry.

Key words: instrumentation: interferometers – techniques: polarimetric – techniques: spectroscopic – stars: magnetic fields

1. Introduction

Stellar magnetic fields are most often observed from the Zeeman splitting of emission or absorption lines where the spectral separation of polarized multiplets is related to the field strength and the degree of polarization to the field orientation. Based on this principle, simultaneous Zeeman spectrometry of sharp spectral lines has successfully determined the intensity of stellar magnetic fields with accuracies which attain a few Gauss (Brown & Landstreet 1981). However, the spectropolarimetric determination of magnetic field geometry is intrinsically difficult because of the small degree of the net detectable polarization due to the integration of the Zeeman effect over the star surface (Borra & Vaughan 1976). In solar- as well as in early-type stars, the existence of symmetrical configurations may cancel the detectable polarization effect although some techniques can partially overcome this handicap. For instance, the Robinson method (Robinson 1980) compares the width of different photospheric lines and the Zeeman-Doppler Imaging (ZDI) technique (Semel 1989; Donati et al. 1989) produces surface maps of solar-type stars restricted to those with noticeable or intermediate $v \sin i$'s. Another alternative solution resides in photometric techniques which study the temporal variation of linear polarization across continuum broad bands (Leroy et al. 1993). In each case, the efficiency of the technique also depends on the intrinsic Doppler-broadening, the chemical peculiarities and generally speaking on the temporal evolution of magnetic structures at the surface of the star.

This paper studies the prospects offered by introducing polarimetric optics in the focal instrument of an optical long baseline interferometer for studying stellar magnetic field geometries. The technique, which we call Spectro- Polarimetric INterferometry (SPIN hereafter), should overcome the shortcomings outlined above thanks to the spatial information of the interferometer. In practice this is done by measuring the interferometer's fringe signal inside linearly and circularly polarized components of a Zeeman multiplet which directly depend on the magnetic topology of the star.

Sect. 2 formulates our simple geometrical model of a magnetic star (an Ap or Bp star for instance) and justifies our simplifying hypothesis. Sect. 3 introduces the Stokes formalism used for describing the Zeeman effect and presents SPIN concept and observables, namely the complex fringe visibilities corresponding to spatial power spectra of the different intensity maps. Numerical results are then presented to illustrate how SPIN can detect and constrain magnetic fields (Sect. 4). A numerical simulation of SPIN sensitivity allows us to give limiting magnitudes in the real case of two optical interferometers: the GI2T-REGAIN and the VLTI for which some potential astrophysical targets are also outlined (Sect. 5). Finally a critical review of the SPIN technique is given in Sect. 6.

2. Model of a magnetic star

To quantitatively evaluate the potential advantage of interferometry for studying stellar magnetic fields, we start with a rather simple magnetic star and focus our effort on characterizing the SPIN observables for such a star and on illustrating SPIN capabilities. More complex geometries demand indeed a more

Send offprint requests to: K. Rousselet-Perraut
Correspondence to: perraut@obs.ujf-grenoble.fr

physically consistent modeling including a radiative transfer treatment of this problem (Chesneau in preparation). The most limiting hypothesis of our first order model are presented and discussed below.

2.1. Geometry and photometry hypothesis

1. Since several Ap stars have $v \sin i \leq 20$ km/s, we assume our model star to be a non-rotating sphere, hence the Doppler broadening of spectral lines is neglected. Although Hubbard & Dearborne (1982) claim that the colatitude-dependent magnetic field could change the radius of Ap stars and the consequent interferometric signal, we do not consider such stellar radius variations in our model since this is not actually supported by observations (Shallis et al. 1985; Leblanc et al. 1994).
2. A second order limb-darkening law is used, using theoretical coefficients taken from a modified ATLAS9 code (Muthsam 1979).
3. Although Ap/Bp stars are known to exhibit chemical inhomogeneities, we assume this to be uniform both in spectral line and continuum over the stellar surface. We thus find ourselves limited to the case of iron lines for which local abundances variations are far smaller than for rare earths, manganese or silicium. Note that this hypothesis is not very restrictive since iron lines are present in all Ap stars.
4. The continuum is assumed to be unpolarized and represents the reference for SPIN calibration measurements.

2.2. Magnetic field description

We consider a magnetic star of radius R, placed at the center of the Cartesian coordinate system *(0, x, y, z)*. The observer is attached to the coordinate system *(0', x', y', z')*. *(Oz)* is the rotation axis of the star and makes an angle β with the magnetic axis *(Oz_M)*. The plane *(Oxz)* includes the line of sight *(Ox')* and the inclination angle i is defined between *(Ox)* and *(Oz')*. At any point M on the star surface the local magnetic field B_M makes an angle γ with the direction **(OM)** (Fig. 1).

We investigate two large scale configurations: a dipolar and a quadrupolar magnetic field. Both are defined in Cartesian set by the polar intensity $Bpol$, as follows (Michaud G. et al. 1981):

$$\mathbf{B_{dip}} = \begin{cases} B_{xd} = 0 \\ B_{yd} = \frac{3}{2} Bpol \frac{yz}{R^5} \\ B_{zd} = \frac{1}{2} Bpol (3\frac{z^2}{R^5} - \frac{1}{R^3}) \end{cases} \quad (1)$$

$$\mathbf{B_{quad}} = \begin{cases} B_{xq} = 0 \\ B_{yq} = \frac{1}{2} Bpol \frac{y}{R^5} (5\frac{z^2}{R^2} - 1) \\ B_{zq} = \frac{1}{2} Bpol \frac{z}{R^5} (5\frac{z^2}{R^2} - 1) \end{cases} \quad (2)$$

with $y^2 + z^2 = R^2$.

2.3. Line profile description

The unperturbed local spectral profile is assumed to be constant. It is a Voigt profile enlarged by a typical 10 000 K thermal Doppler effect. The damping constant is chosen to correspond to iron atoms. The line profile Equivalent Width (EW) is a parameter of the model (Table 1).

The split line is assumed to be a Zeeman triplet and is considered isolated (i.e not blended). Line blends depend upon the Doppler shift and will be considered in further works for faster rotators (Chesneau in preparation).

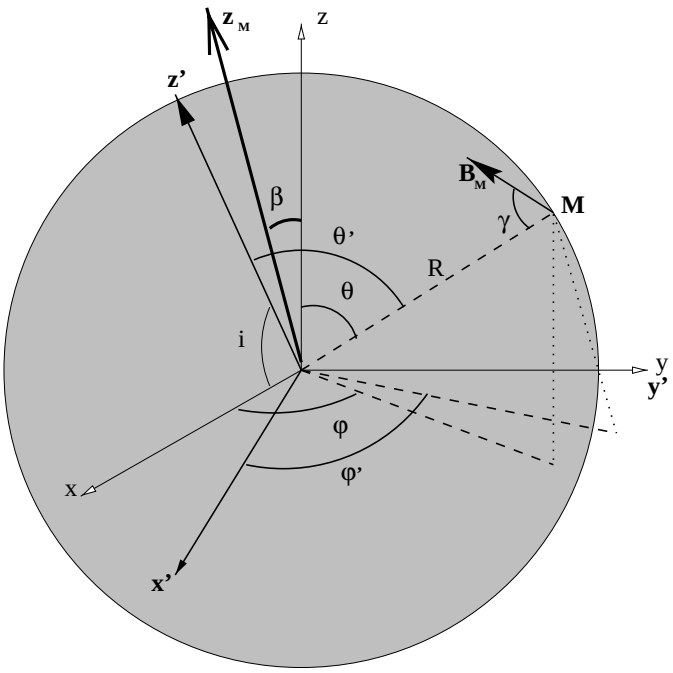

Fig. 1. Coordinate system defining the geometry used for modeling the magnetic star: R is the photospheric disk radius, γ the angle between the local magnetic field B_M and the direction OM for a point M sitting at *(x, y, z)*, and β is the angle between the rotation axis *(Oz)* and the magnetic axis *(Oz_M)*.

2.4. Instrumental hypothesis

The spectropolarimeter instrumental profile is assumed to be Gaussian with a Full Width Half Maximum (FWHM) equal to the resolution element. This resolution element is sampled by two pixels of the detector with respect to the Shannon criterion. The photo-counting camera is supposed to be perfect.

2.5. Numerical code parameters

The parameters of the numerical code are summarized in Table 1. For the following simulations we consider a *prototype* Ap star whose characteristics are given in Column 3 of Table 1.

3. Basic concept and observables of SPIN

3.1. Zeeman effect formalism and intensity maps

For a magnetically sensitive spectral line with a triplet Zeeman pattern, the separation between the components is given by:

$$\Delta\lambda = 4.67.10^{-13} {\lambda_o}^2 gB \quad (3)$$

Table 1. Parameters of the numerical code for SPIN and characteristics of the prototype star. See text for the meaning of B and BN.

Symbol	Item	Prototype star	Range
Φ	Stellar angular diameter	0.7 mas	
$Bpol$, g	Polar field, Landé factor	$g.Bpol$ = 4 000 G	
T_O	Effective temperature	12 000 K	
λ_0	Central wavelength	0.6 μm	
EW	Equivalent Width of the line profile	90 mÅ	
i	Inclination		[0°; 90°]
β	Obliquity		[0°; 90°]
ω	Stellar phase		[0°; 360°]
R	Spectral resolution	30 000	up to 60 000
BN	Baseline orientation		[0°; 90°] (*)
B	Baseline length	50 m; 100 m	[0 m; 200 m]

(*) 0° corresponds to a North-South orientation and 90° corresponds to a West-East one.

where λ_o is the central wavelength of the line (in Å), g the Landé factor and B the magnetic field intensity.

By denoting f_λ the local line profile and λ_o the central wavelength, the Zeeman effect at any point M is characterized by a Stokes vector proportional to (Collett 1993):

$$\mathbf{S}_{\lambda \mathbf{o}} = f_{\lambda_o - \Delta\lambda} \begin{bmatrix} 1+\cos^2\gamma \\ -\sin^2\gamma \\ 0 \\ -2\cos\gamma \end{bmatrix} + f_{\lambda_o} \begin{bmatrix} 2\sin^2\gamma \\ 2\sin^2\gamma \\ 0 \\ 0 \end{bmatrix} + f_{\lambda_o + \Delta\lambda} \begin{bmatrix} 1+\cos^2\gamma \\ -\sin^2\gamma \\ 0 \\ 2\cos\gamma \end{bmatrix} \quad (4)$$

The σ-components at $\lambda_o \pm \Delta\lambda$ are elliptically polarized of opposite polarities. Both σ-components contain circular components whose intensities are $I_{\sigma_+} = (1+\cos\gamma)^2$ and $I_{\sigma_-} = (1-\cos\gamma)^2$ respectively. The π-component at λ_o is linearly polarized with an intensity $I_\pi = 2\sin^2\gamma$. For γ=0°(*longitudinal* Zeeman effect), only the σ-components exist and are left and right circularly polarized. For γ=90°(*transverse* Zeeman effect), the three components are linearly polarized (since the σ-components ellipticities are null) and the σ- and π-polarizations are crossed.

After a classical analyzer of linear polarizations, the intensity map is:

$$I_{lin}(\lambda) = (f'_{\lambda_o - \Delta\lambda} + f'_{\lambda_o + \Delta\lambda})\cos^2\gamma + f'_{\lambda_o} I_\pi \quad (5)$$

After a classical analyzer of circular polarizations, the intensity maps are:

$$I_{right}(\lambda) = f'_{\lambda_o - \Delta\lambda} I_{\sigma_-} + f'_{\lambda_o} I_\pi + f'_{\lambda_o + \Delta\lambda} I_{\sigma_+} \quad (6)$$

$$I_{left}(\lambda) = f'_{\lambda_o - \Delta\lambda} I_{\sigma_+} + f'_{\lambda_o} I_\pi + f'_{\lambda_o + \Delta\lambda} I_{\sigma_-} \quad (7)$$

where f'_λ denotes the local line profile convolved with the instrumental one (See Sect. 2.4). Contrary to classical spectro-polarimetry, such a *local* convolution is required to produce intensity maps at various wavelengths (Fig. 2).

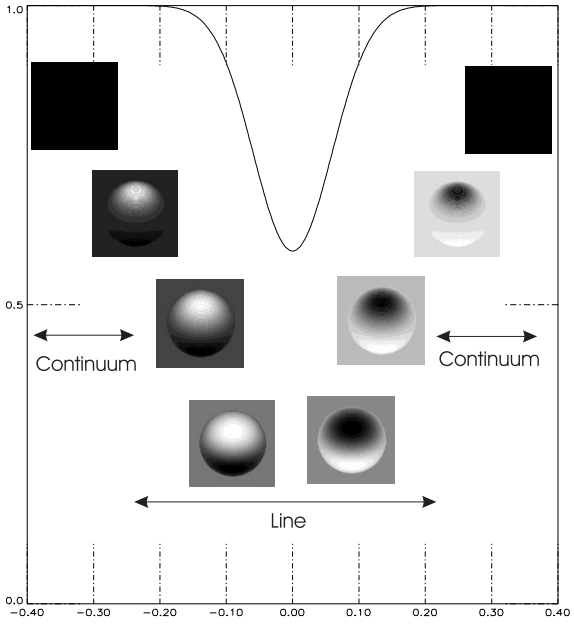

Fig. 2. $I_{right}(\lambda) - I_{left}(\lambda)$ intensity maps along a line for 0.2 Å channels. R = 60 000 and $i = 60°$. The local polarization rate reaches 30% for the central pixels, 7% for the neighboring ones, and is negligible for the others.

3.2. SPIN concept and observables

A two-telescope interferometer can sample the spatial power spectrum (Fourier transform) $|\widetilde{O}|e^{i\psi}$ of sky brightness O(α, δ) at the spatial frequency **B**/λ. **B** stands for the interferometric baseline vector projected on the sky and λ the mean wavelength at which the interferometer operates (Born & Wolf 1984). Thus:

$$\mathbf{V}(\mathbf{B}/\lambda) \propto |\widetilde{O}(\mathbf{B}/\lambda)| e^{i\psi(\mathbf{B}/\lambda)} \quad (8)$$

Hereafter we call *visibility* V(**B**/λ) the modulus $|\widetilde{O}(\mathbf{B}/\lambda)|$ normalized at the null spatial frequency and *fringe phase* ψ(**B**/λ).

An interferometer equipped with a classical spectro-polarimeter measures the linear and circular visibilities V_{lin}(**B**/λ), V_{right}(**B**/λ), and V_{left}(**B**/λ) which are directly linked to the Fourier transform of $I_{lin}(\lambda)$, $I_{right}(\lambda)$, and $I_{left}(\lambda)$, respec-

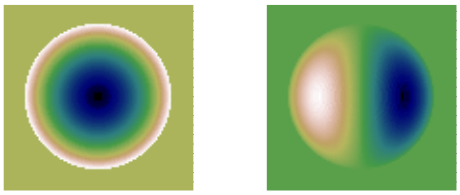

Fig. 3. $I_{right}(\lambda) - I_{left}(\lambda)$ intensity maps for a pole-on dipole (left) and an edge-on dipole (right). BN = 90°, R = 60 000 and $g.Bpol$ = 4 000 G.

tively. SPIN observations of magnetic stars thus provide various polarized visibilities as a function of baseline length B, baseline orientation BN and wavelength λ.

Fringe phase information ψ is inaccessible with a two-telescope interferometer. However, if one can record the interferometric signal simultaneously at two neighboring wavelengths, one can retrieve positional information on the sky brightness at a given wavelength λ_1 relative to the second λ_2 provided the object under observation remains unresolved at one of the wavelengths. In other words:

$$\psi = 2\pi \frac{B}{\lambda} \epsilon \tag{9}$$

where ϵ is the projection of the vector distance $(\Delta\alpha, \Delta\delta) = (\alpha, \delta)_{\lambda_1} - (\alpha, \delta)_{\lambda_2}$ on the interferometer's baseline. α and δ are the object's position on the sky at λ_1 and λ_2. A fringe phase variation thus directly traduces a displacement of the star photo-center. It is theoretically known (Petrov 1988) and practically demonstrated (Vakili et al. 1997) that the measurable ϵ can be much smaller than the angular resolution of the interferometer λ/B.

In the following, we use this *differential interferometry* technique to compute fringe phases as well as visibilities (Berio et al. 1999). Thus both SPIN observables are obtained by an inter-correlation method between a large continuum channel and the narrow channel in the spectral line (Fig. 2). Such a differential technique allows to improve the sensitivity of the technique (Petrov et al. 1986).

4. Numerical results of SPIN capabilities

4.1. Diagnosis on magnetic field configurations

To illustrate the SPIN observables behavior, we first present two extreme cases: a pole-on dipole ($\langle B_z \rangle \sim \frac{B_{pol}}{4}$) and an edge-on dipole ($\langle B_z \rangle = 0$) (Fig. 3). In the first case, the polarized light modulates the intensity distribution and mimics a strong limb-darkening. As a consequence, the star appears larger/smaller in the polarized lines than in the unpolarized continuum, inducing a strong visibility variation. Both polarized and unpolarized light distribution are centro-symmetric and no phase effect is expected between them. For the edge-on dipole, this situation is inverted. The longitudinal field is minimum and consequently the visibility is less affected by polarized light. In this case, since the configuration is highly anti-symmetric, a large phase effect can occur. The detections will take place between these extreme cases. The inverted behavior between visibility and fringe phase is obviously the key point to strongly constrain both i and β.

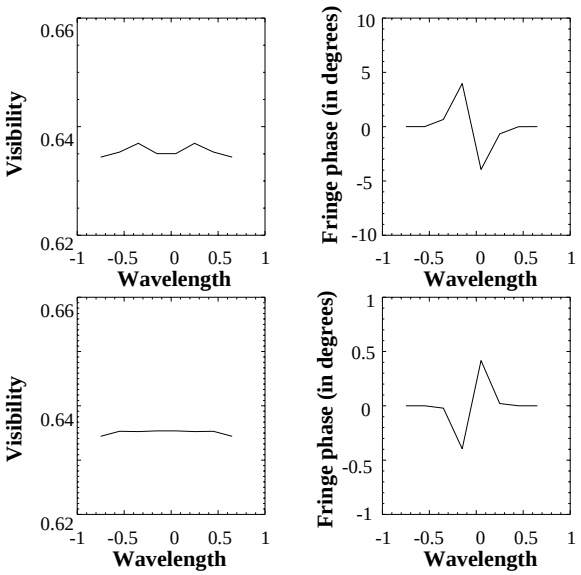

Fig. 4. Circular visibility and fringe phase for an edge-on dipole (up) and an edge-on quadrupole (down) versus wavelength. 0 denotes the central wavelength and each point corresponds to a resolution element. $g.Bpol$ = 4 000 G.

4.1.1. Symmetric configurations

To point out the spatial resolution capabilities of SPIN, we study two symmetric configurations where the classical mean longitudinal field $\langle B_z \rangle$ equals zero: an edge-on dipole and an edge-on quadrupole.

For these cases, the longitudinal field is minimum and therefore the visibility signal is minimum too (Fig. 4). However, for the edge-on dipole, the photo-center displacement induced by the polarized light is maximum and compensates for the decrease of polarization rate: a phase signal is detectable. The quadrupole configuration also creates a polarized anti-symmetry and a phase signal could be detectable. Note that we assume the baseline orientation BN perpendicular to the axis of anti-symmetry, which induces a maximum signal.

4.1.2. SPIN baseline effects and magnetic field orientation

Visibilities and phase fringes have been computed for various magnetic configurations, the main parameters being $i, \beta, g.Bpol$ and BN. For convenience and since we aim at illustrating SPIN observables, we assume that the axes *(Oz_M)*, *(Oz)* and *(Oz')* are coplanar, which implies that only the angle $i + \beta$ can be constrained (See Sect. 6 for more general cases). The following example takes $g.Bpol$ = 4 000 G (Figs. 5- 6). The resulting accuracies on visibility and phase are similar for other realistic $g.Bpol$ values.

Visibilities versus spatial frequency (i.e. baseline length) show a very slight dependence on magnetic field orientation

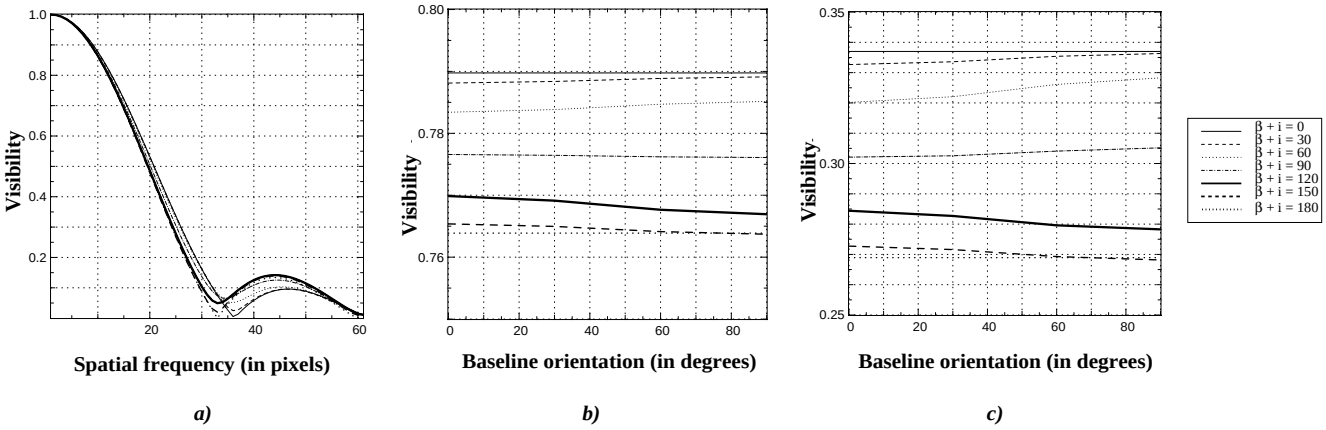

Fig. 5a–c. Circular visibility for various angles $i + \beta$ and $g.Bpol$ = 4 000 G. **a** versus spatial frequency (in pixels) for BN = 90°. **b** versus baseline orientation BN for a baseline of 50 m. **c** versus baseline orientation BN for a baseline of 100 m.

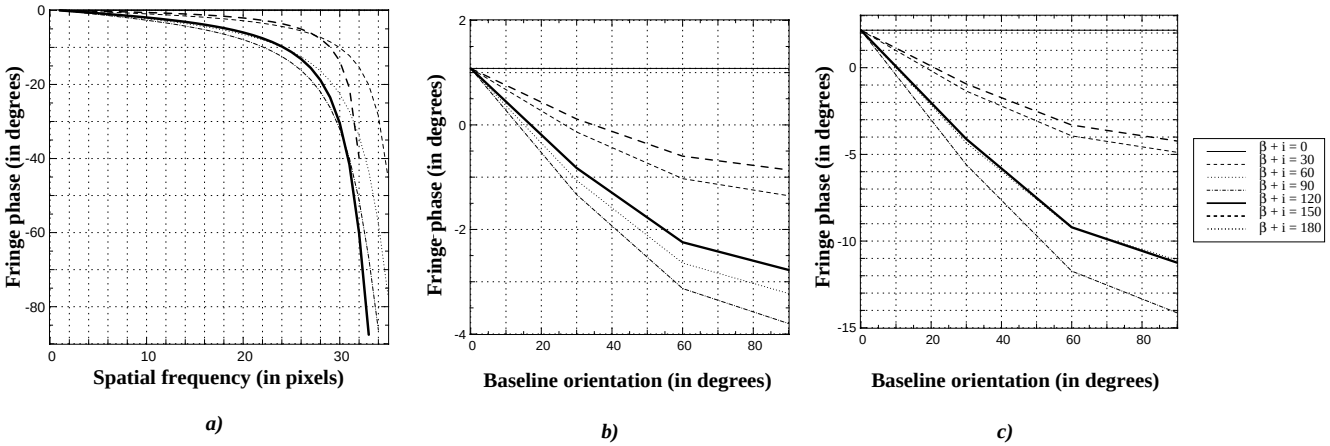

Fig. 6a–c. Circular fringe phase (in degrees) for various angles $i + \beta$ and $g.Bpol$ = 4 000 G. **a** versus spatial frequency (in pixels) for BN = 90°. **b** versus baseline orientation BN for a baseline of 50 m. **c** versus baseline orientation BN for a baseline of 100 m.

$i+\beta$ (Fig. 5a): the larger visibility differences occur at large spatial frequencies for very small visibilities ($\leq$10%). For smaller baselines, the required absolute visibility accuracy is as small as 0.1%: for $30° \leq i + \beta \leq 150°$, such an accuracy allows to constrain $i + \beta$ with an accuracy of few degrees if the baseline equals 100 m (Fig. 5c) and of 10-15° if the baseline equals 50 m (Fig. 5b).

On the contrary, fringe phases versus spatial frequency significantly vary with $i + \beta$ (Fig. 6a). Fringe phases also depend upon the baseline orientation BN (Fig. 6b-c): these variations can reach 15° for a baseline of 100 m and 5° for a baseline of 50 m. The accuracy on $i + \beta$ strongly depends upon $i + \beta$ and BN: it can be better than 5° for a baseline of 100 m and a high phase accuracy of 0.1°. For a realistic phase accuracy of 0.5°, $i + \beta$ can be constrained within 8-10° for a baseline of 100 m and within 15° for a baseline of 50 m. Figs. 6b-c also demonstrate the great interest of simultaneous different baseline orientations and multi-telescope arrays for avoiding to confuse different $i + \beta$ (See Sect. 6.2.3).

As each baseline length produces independent measurements, the accuracy on $i + \beta$ can be improved by a factor $\sqrt{N}$ if N is the number of measurements.

4.1.3. Oblique rotator and temporal variability

Temporal variations of visibility and fringe phase are reported in Figs. 7 and 8 for various configurations of i and β. These variations can be detected even with a baseline of 50 m since they exceed few degrees for the fringe phase (and up to 30° for B = 100 m) and few percents for the visibility. For a given i, the variation amplitudes of the visibility and fringe phase increase with β. Besides, for a given angle $i + \beta$ (constrained in Sect. 4.1.2), the variation amplitude of the fringe phase increases when i decreases, allowing to independently constrain i and β.

4.2. Small field detection

For a given visibility and fringe phase accuracy, what is the minimal magnetic field that SPIN can detect? Fig. 9 reports the visibility and phase versus $Bpol$ (g = 2) for different baselines and pole-on (visibility only as explained in Sect. 4.1.1) and edge-on configurations.

For the pole-on configuration, considering a spectral resolution R = 30 000 and a 1% visibility accuracy, no signal can be detected with a 100 m baseline for $Bpol \leq$ 2000 G. With B =

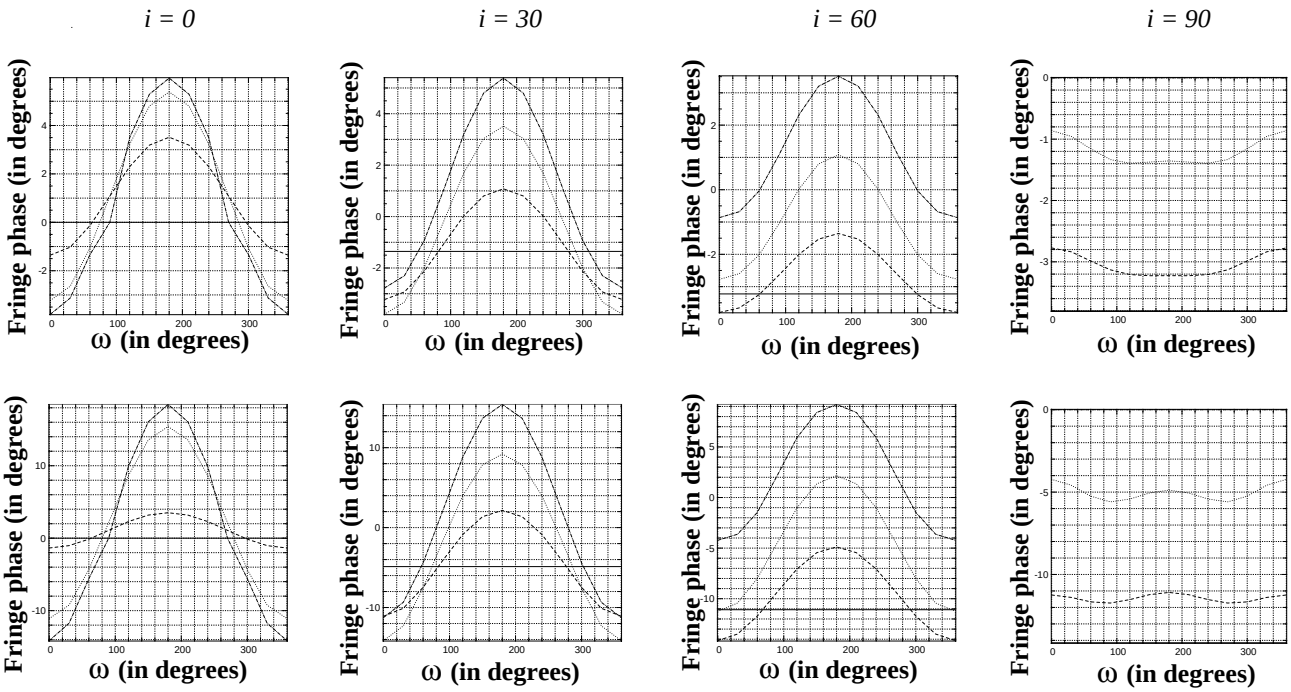

Fig. 7. Circular fringe phase (in degrees) for various angles β versus stellar phase ω. BN = 90° and $g.Bpol$ = 4 000 G.β equals 0° (solid line), 30° (dashed line), 60° (dotted line) and 90° (dash-dotted line). The inclination i equals 0°, 30°, 60° and 90° from left to right. The baseline equals 50 m (top) and 100 m (bottom).

200 m, a polar field of 1200 G can be detected. For an visibility accuracy of few tenths percents, $Bpol$ of few hundreds Gauss can be detected even for B = 100 m.

For the edge-on configuration, a huge phase effect occurs with B = 200 m baseline but it must be pointed out that the signal detection is much more difficult with this baseline since the visibility is very low (the first zero visibility for a 0.7 mas star is 215 m). Nevertheless, we can detect $Bpol$ as low as 250 G with a very pessimistic 5° phase accuracy and $Bpol$ of about 100 G for a realistic 1° phase accuracy.

Generally, a spectral resolution of 30 000 is not sufficient to detect small magnetic fields and baselines larger than 150 m are mandatory. With R = 60 000, such a detection becomes possible with shorter baselines even with the visibility signal.

To conclude the sensitivity difference between visibility and phase signal implies very different magnetic field detection thresholds. An edge-on configuration will be detected much easier than pole-on configuration, contrary to classical methods.

4.3. Transverse field measurements

In spectropolarimetry, the mean longitudinal field $\langle Bz \rangle$ is generally not sufficient to determine the surface field, but attempts to observe the transverse Zeeman effect are scarce. Since each Zeeman component produces opposite linear polarizations, a large cancellation occur and very high spectral resolutions and/or sensitivities are required (Borra & Vaughan 1976). The same difficulties arise for SPIN and the question is to determine whether this sensitivity loss can be counterbalanced by the spatial resolution.

The first result is that the visibility signal is strongly attenuated and a spectral resolution $R \geq 60000$ are mandatory in the visible. The phase signal is unfortunately also strongly attenuated due to the high symmetry of the transverse intensity maps whatever the inclination i and even for spectral resolutions higher than 60 000.

To conclude, it does not seem interesting to measure the transverse field with SPIN. Note that, with several baselines, the longitudinal detections should be sufficient to retrieve the field geometry.

5. Numerical simulation of SPIN sensitivity

5.1. Instrumental requirements

In principle there is no obstacle to equip the focal instrument of an interferometer by polarimetric optics. A simple polarization state analyzer using a Wollaston prism and quarter-wave plates at 45°can perfectly match the specifications for calibration and visibility determination in the different Zeeman components.

The difficulty of SPIN is due to the optical complexity of interferometers in general which demands numerous and stringent calibrations of internal polarization to attain the desired and unbiased accuracies to determine stellar magnetisms. Visibility accuracies of few tenths of percent are required to constrain magnetic field orientations. Such accuracies are reached with the FLUOR instrument thanks to spatial filtering and simultaneous photometric calibration (Coudé du Foresto et al. 1997) and such performances are expected for the focal instrument AMBER of the VLTI (Petrov et al. 1998). The previous study

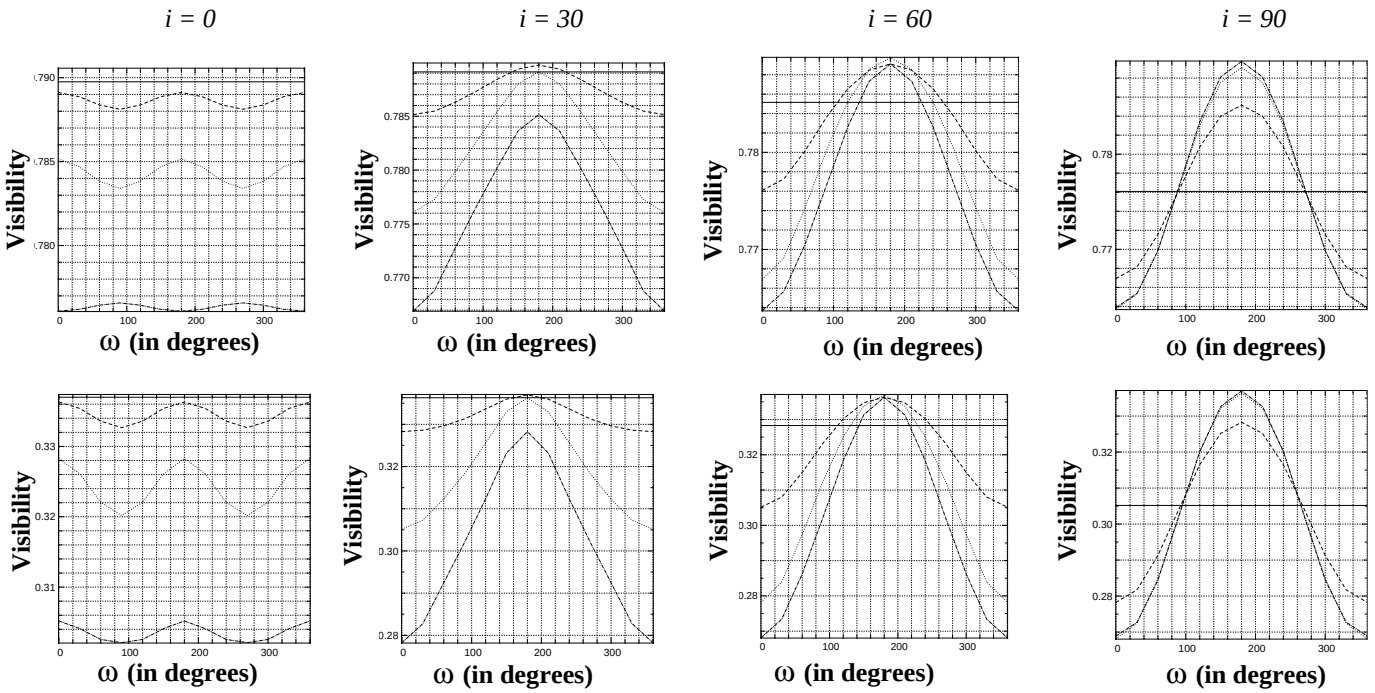

Fig. 8. Circular visibility (in degrees) for various angles β versus stellar phase ω. BN = 90° and $g.Bpol$ = 4 000 G. β equals 0° (solid line), 30° (dashed line), 60° (dotted line) and 90° (dash-dotted line). The inclination i equals 0°, 30°, 60° and 90° from left to right. The baseline equals 50 m (top) and 100 m (bottom).

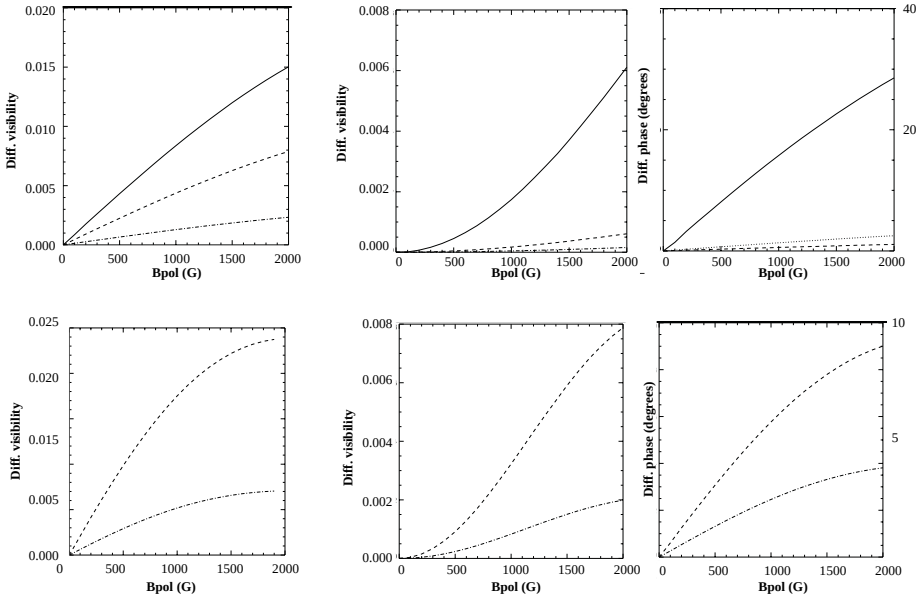

Fig. 9. Differential circular visibility and fringe phase between the two central pixels for a pole-on (left) and an edge-on (middle and right) dipole versus $Bpol$ (g = 2) for R = 30 000 (up) and R = 60 000 (down). The baseline B equals 50 m (dash-dotted line), 100 m (dashed line) or 200 m (solid line).

also demonstrates that fringe phase constitutes a powerful tool for constraining magnetic fields provided that the phase accuracy reaches few tenths of degree. Such accuracies have already been obtained with the GI2T interferometer (Vakili et al. 1997) and accuracies better than 0.1° are expected with AMBER.

Baselines longer than 50 m are mandatory for partially resolve Ap and Bp stars, which is reachable with existing interferometers (GI2T for instance) and a fortiori with foreseen ones (VLTI).

SPIN technique obviously implies a spectrometric device with high spectral resolution (at least 30000 in the visible and 10000 in the near-infrared). Nowadays only the GI2T/REGAIN (Mourard et al. 1998) is equipped with such a device in the visible range and AMBER, which is first restricted to the near-infrared range (J, H and K bands), is foreseen with a spectrometric mode. As regards to polarimetric devices, only REGAIN on the GI2T includes such a facility. AMBER is first restricted to a linear polarizer (Malbet 1999).

Finally, three or more baselines appear to significantly improve the SPIN performances by allowing to avoid confusion between various magnetic field configurations. This facility is currently available on two existing arrays, COAST (Baldwin et al. 1996) and NPOI (Benson et al. 1997), and will be accessible with the future instruments such as the VLTI (Mariotti et al. 1998) or CHARA (McAlister et al. 1998).

5.2. Limiting magnitudes

As regards to the previous instrumental considerations, we have computed SPIN sensitivity for two realistic interferometric configurations. First we contemplate SPIN validation with the existing GI2T/REGAIN instrument since it has a maximal single baseline of 65 m and besides it is designed with a spectro-polarimetric device whose spectral resolution reaches 30000. Then we obviously foresee observations with the ESO VLTI interferometer composed by four *fixed* 8m-Unit Telescopes (UT) with baselines from 40 m to 100 m and three (and more) *movable* 1.8m-Auxiliary telescopes (AT) with baselines reaching 200 m.

5.2.1. GI2T

All the system being already designed, a global simulation of the GI2T/REGAIN is possible and thus our computation of SPIN performances on the GI2T is very accurate (Berio et al. 1999). The inter-correlation estimator is defined in the spectral density space and is thus quadratic. The photon noise is assumed to be the single limitation. For fringe phase computation, neither geometrical variability nor flux limitation by neutral densities have been taken into account, inducing an under-estimation for the smallest magnitudes.

For a Fried parameter of r_0 = 7 cm, an exposure time τ = 20 ms, a number of recorded images N_i = 90 000, a science channel of 0.2 Å large, a continuum channel of 20 Å large and without adaptive optics, the expected SNR of the squared visibility and the phase errors are given in Fig. 10 when observing in SPIN mode. The accuracies required for SPIN are reached for $m_V \leq 2$. These performances will be greatly improved with adaptive optics (Vérinaud et al. 1998) which will focus the coherent signal and increase the SNR: m_V reaches 6.

5.2.2. VLTI

Our computation of SPIN performances on the VLTI is based on the expected performances of the AMBER focal instrument (Malbet 1999). With the higher spectral resolution R = 10 000, an elementary exposition time τ = 100 s, a total integration time of 4 hours, a visibility signal-to-noise SNR = 100, the AMBER expected limiting magnitudes are m_J = 5.8, m_H = 10.8 and m_K = 12.3 on the UTs with fringe tracking and adaptive optics in average atmospheric conditions. These performances are quite identical in the H and K bands with the ATs thanks to more efficient adaptive optics. Within the context of SPIN applications, note that considering R = 10 000 in the near-infrared is equivalent to R = 30 000 in the visible (Eq. 3), even if in terms of spatial resolution, this infrared spectral range requires longer baselines (Sect. 5.3). To conclude, considering for SPIN an instrumental throughput twice lower than AMBER one (due to polarimetric equipment) and a shorter total integration time (to preserve temporal evolution studies) leads to satisfying limiting magnitudes in the H and K bands whatever the VLTI configuration (UTs or ATs).

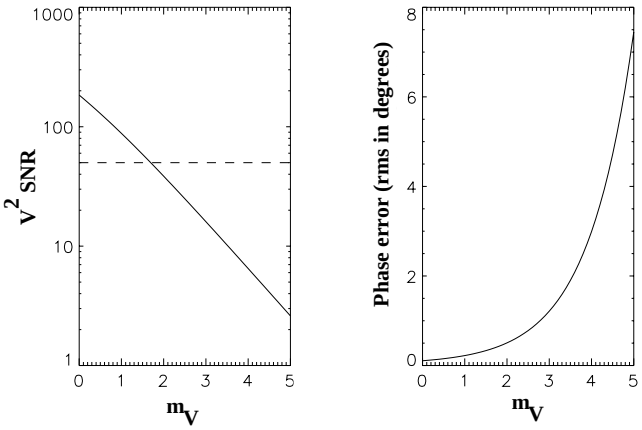

Fig. 10. SNR of the squared visibility (left) and phase error due to speckle and photon noise (right) versus stellar magnitude. The dashed line indicates the 1% accuracy threshold.

5.3. Astrophysical candidates

In a first step, the targets have to be close (i.e bright) and strongly magnetized. The main limitation is clearly the angular diameter since Ap stars radius is about 2-4 solar radius. With the 60 m baseline of the GI2T/REGAIN, a few well known stars will be considered: αCVn (m_V = 2.9, ϕ = 0.88 mas, Shallis et al. 1985) and βCrB (m_V = 3.9, ϕ = 1 mas, Wade 1997) for the magnetic ones. ϵUma (m_V = 1.8, ϕ = 1.5 mas, Shallis & Blakwell 1979) and α And (m_V = 2.1, ϕ = 1.25 mas, Shallis et al. 1985) that are weakly magnetized should also be investigated.

For the VLTI, the same considerations apply and the AT telescopes offer both large baselines and a great coverage of the spatial frequencies. The potential targets for VLTI are more numerous in the visible considering the 200 m baseline and the greater limiting magnitude. With a limiting angular diameter ϕ_{lim} of 0.25 mas (and $m_V \sim 6$), about 50 stars could be observed in the visible and a dozen in J, H and K bands ($\phi_{lim} \sim$ 0.6 mas).

6. Discussion

6.1. Stellar rotation axis

In our computations, the rotation axis is chosen as a reference and its orientation relative to the sky θ_i is supposed to be known. However, this angle has to be found since no indication from classical methods are available except for $v \sin i$ informations and for the case of Be stars whose disks greatly influence the polarization angles of the light. For Ap stars, interferometry in

natural light (See Sect. 6.2.2) can provide this information. This could be done considering the Doppler effect on the phase due to the star rotation (Chalabaev 1992). But this method requires high phase accuracy and high $v \sin i$, larger than those considered in this work. The best way is to use temporal evolution and phase closure to constrain β, i and θ_i.

6.2. SPIN data processing

6.2.1. SPIN calibrators

Unlike traditional polarimetric methods, standard polarimetric stars cannot always be interferometric references. This is due to the spatial resolving property of stellar interferometers: if for reasons of symmetry the photo- polarimetric signature of a star is null, it can still produce a spatial signal. Therefore a SPIN calibration star can be either a calibration star that is unresolved at the angular resolutions achieved by the interferometer, or the observed object itself at a spatial frequency where it is unresolved. The most critical instrumental calibrations concern the oblique reflections inside the interferometric arms (Rousselet-Perraut et al. 1997a). It is also preferable to record polarized interferograms simultaneously on the same panoramic detector and to switch the polarization states of the analyzer to unbias the visibilities from detector response.

6.2.2. Calibrations by observations in natural light

Like in spectropolarimetry, SPIN measurements in different states of polarization should be sandwiched between interferometric data in natural light on the star itself, compared in turn to an unresolved calibrator, the process being repeated for increasing and orientation-changing baselines (Rousselet-Perraut et al. 1997b). In fact, our differential method to recover SPIN signal isolates the Zeeman effect as the single origin of polarization change in the line but a signal comparison, between the continuum and the line in natural (i.e. non polarized) light, is mandatory to extract information about other unpolarized effects.

First, observations in natural light allow to disentangle geometrical effects since interferometry is very sensitive to the spatial shapes of the star. These observations can be a useful tool for Ap stars where atmospheric distortions and radius variations following the magnetic field structure are suspected (Hubbard & Dearborne 1982). These phenomena can induce a temporal variation of the surface and shape of the visible face of the star which can modify the interferometric signal. Nevertheless, the radius variation could at the best be of the order of few percents (Stepien 1978; Leblanc et al. 1994) and is the same at all wavelengths, which does not affect our differential signal.

In the same way, a patchy intensity distribution will create a complex and time dependent signal. Ap stars are chemically peculiar stars and the studied line can present a very different intensity distribution from the continuum. The signal differences between the continuum and the lines in polarized light has to be corrected for the differences existing in natural light.

The SPIN study of Ap star implies indeed an important by-product of intensity distribution and/or geometric information of great interest.

6.2.3. SPIN inversion

As previously illustrated, SPIN can provide visibilities and fringe phases for various Zeeman components, various temporal phases ω, various baseline lengths B and orientations BN when more than three telescopes are used. These visibility points are directly linked to the object intensity distribution (Eq. 8) and can provide spatial, spectral and temporal information about stellar magnetism. Especially, they can bring constraints on stellar parameters such as i, β and θ_i. Even if astrophysical information can be obtained by model fitting, to constitute a very powerful means of diagnosis for stellar magnetism, SPIN obviously requires an efficient inversion method allowing to converge on a star model from various complementary observables.

7. Conclusion and perspectives

SPIN (Spectro-Polarimetric INterferometry) method is a new and complementary way to study stellar magnetic fields. First we only investigate slow rotators (i.e. $v \sin i \leq 20$ km/s) whilst the Zeeman Doppler Imaging (ZDI) deals with stars which exhibit sufficient $v \sin i$ (≥ 30 km/s). Further works will investigate the case of faster rotators by including Doppler effect in our model. In this case, Doppler effect can eventually emphasize the local magnetic fields, which could be detected by the SPIN technique that presents the unique and strong advantage of providing spatial information for the Zeeman components.

A simple analytical model of magnetic stars allows us to illustrate the SPIN capabilities for detecting and constraining magnetic fields. The fringe phase appears to be the most powerful observable and requires accuracies better than 0.5°. Thus only very bright stars ($m_V \leq 2$) can be observed using SPIN techniques on presently operating instruments. In a near future, the operation of the 8m-telescopes and 1.8m-telescopes equipped with performant adaptive optics of the VLTI will allow to reach limiting magnitudes $m_K \leq$ 8-10 and to foresee a larger sample of objects for SPIN technique. Such objects also require milli-arcsecond angular resolutions (hence baselines of several tens meters) and a multi-element interferometer with 2D imaging capabilities for getting unambiguous pictures of the stellar magnetic field geometry. Within this interferometric short-term context, we advocate that a polarimetric device implemented on the AMBER visible extension would be a powerful means for studying stellar magnetism and others phenomena of stellar polarization (scattering,...).

Finally it must be emphasized that SPIN observations may undoubtedly lead to misguiding pitfalls if, for the very first observations, they are not accompanied by more classical and mature techniques like ZDI. It is even mandatory that any SPIN attempt should be accompanied by simultaneous spectro-polarimetric observations to independently constrain the magnetic source. Starting with well-known magnetic stars must be the

starting point with the hope that sooner or later all potentially magnetic stars will be truly imaged by arrays of optical telescopes.

Acknowledgements. The authors are grateful to J. Bouvier, D. Mourard and G. Mathys for their readings and comments of the original and revised manuscripts. They want to thank the referee Dr. M. Semel for his constructive criticisms, which allowed us to improve the paper. We would like to thank C. Stehlé and N. Thureau for fruitful discussions.

References

Baldwin J.E., Beckett M.G., Boysen R.C., et al., 1996, A&A 306, L13
Benson J.A., Hutter D.J., Elias N.M., et al. 1997, Astronomical Journal 114, 1221
Berio P., Mourard D., Bonneau D., et al., 1999, Journal of Optical Society of America A Vol. 16, 4
Born M., Wolf E., 1984, Principles of optics. Pergamon Press, New York
Borra E.F., Vaughan A.H., 1976, ApJ 210, L145
Brown D.N., Landstreet J.D., 1981, AJ 246, 899
Chalabaev A., 1992, hrii.conf, 403
Chesneau O., in preparation
Collett E., 1993, Polarized light - Fundamentals and applications. Marcel Dekker, New York
Coudé du Foresto V., Ridgway S.T., Mariotti J.-M., 1997, A&AS 121, 379
Donati J.F., Semel M., Praderie F., 1989, A&A 225, 467
Hubbard E.N., Dearborne D.S.P., 1982, ApJ 254, 196
Leblanc F., Michaud G., Babel J., 1994, ApJ 431, 388
Leroy J.L., Landolfi M., Landi Degl'Innocenti E., 1993, A&A 270, 335
McAlister H.A., Bagnuolo W.G., Ten Brummelaar T.A., et al., 1998, In: Reasenberg R.D. (ed.) Proc. SPIE 3350, Astronomical Interferometry. p. 947
Malbet F., 1999, AMBER the near-infrared interferometric instrument. ESO/VLTI Conceptual Design Review
Mariotti J.-M., Denise C., Derie F., et al., 1998, In: Reasenberg R.D. (ed.) Proc. SPIE 3350, Astronomical Interferometry. p. 800
Michaud G., Charland Y., Megessier C., 1981, A&A 103, 244
Mourard D., Thureau N., Antonelli P., et al., 1998, In: Reasenberg R.D. (ed.) Proc. SPIE 3350, Astronomical Interferometry. p. 517
Muthsam H., 1979, A&AS 35, 107
Petrov R.G., Roddier F., Aime C., 1986, JOSA A, Vol. 3, n°5, p. 634
Petrov R., 1988, In: Merkle F. (ed.) High-Resolution Imaging by Interferometry. ESO Conference, March 1988, Garching, Germany, p. 235
Petrov R.G., Malbet F., Richichi A., et al., 1998, The Messenger 92, p. 11
Robinson R.D., 1980, ApJ 239, 961
Rousselet-Perraut K., Vakili F., Mourard D., 1997a, Optical Engineering Vol. 36(4), 980
Rousselet-Perraut K., Vakili F., Mourard D., et al., 1997b, A&AS 123, 173
Semel M., 1989, A&A 225, 456
Shallis M.J., Blakwell D.E., 1979, A&A 79, 48
Shallis M.J., Booth A.J., Baruch J.E.F., et al., 1985, MNRAS 213, 307
Stepien K., 1978, A&A 70, 509
Vakili F., Mourard D., Bonneau D., et al., 1997, A&A 323, 183
Vérinaud C., Blazit A., Berio P., et al., 1998, In: Catching the perfect wave, in press
Wade G.A., 1997, A&A 325, 1063